

Technical note

Evidence of the coexistence of upstream and downstream solitary wavetrains in the real atmosphere

QUANAN ZHENG^{†*}, SAMUEL S. P. SHEN[‡], YELI YUAN[§],
NORDEN E. HUANG[¶], V. KLEMAS[†], XIAO-HAI YAN[†],
FENGYAN SHI^{††}, XUEBIN ZHANG[†], ZHONGXIANG ZHAO[†],
XIAOFENG LI^{‡‡} and P. CLEMENTE-COLÓN^{‡‡}

[†]Department of Meteorology, University of Maryland, College Park,
Maryland 20742, USA

[‡]Department of Mathematical Sciences, University of Alberta, Edmonton,
Alberta, Canada T6G 2E1

[§]The First Institute of Oceanography, SOA, Qingdao, Shandong, China

[¶]Ocean & Ice Branch, NASA Goddard Space Flight Center, Greenbelt,
Maryland 29771, USA

^{††}Center for Applied Coastal Research, Department of Civil Engineering,
University of Delaware, Newark, Delaware 19716, USA

^{‡‡}NOAA/NESDIS, E/RA3, Room 102, WWBG, 5200 Auth Road,
Camp Springs, Maryland 20746-4304, USA

(Received 8 April 2003; in final form 5 August 2003)

Abstract. From a true colour image of the Sea-viewing Wide Field-of-view Sensor (SeaWiFS) onboard the Orbview-2 satellite, we observed two packets of orderly wave clouds on two sides of Hainan Island in the South China Sea. A packet of 23 wave clouds stretches southward from the island. A second packet of more than 20 wave clouds stretches north-eastward off the north-east coast of the island. The concave orientation of the wave cloud lines implies that both packets are propagating away from the island. A chart of geopotential height and velocity at 850 mbar shows a south-westerly air flow over the island; hence the two wave cloud packets propagate upstream and downstream, simultaneously. Thus, we have found new evidence of the coexistence of both upstream and downstream solitary wavetrains generated in the real atmosphere by land topographic disturbances. Comparison with theoretical results supports this conclusion.

1. Introduction

In recent years, solitary wave packets (Zheng *et al.* 1998a), mountain waves (Eckermann and Preusse 1999), coastal lee waves (Zheng *et al.* 1998b; Li *et al.* 2001), island lee waves (Vachon *et al.* 1994), gravity waves (Chunchuzov *et al.*

*Corresponding author; e-mail: quanan@atmos.umd.edu

2000), vortex streets (Li *et al.* 2000) and upstream wave packets (Li *et al.* 2004) in the atmosphere have all been identified from satellite images. Most of these waves are generated by airflow over a topographic (or dynamical) obstacle, constitute a single wave packet, and propagate in one direction only. Theories developed by Grimshaw and Smyth (1986), Wu (1987) and Shen (1993), among others, however, predicted that perturbation of a topographic obstacle could generate two separate wave packets arranged on two sides of the obstacle. Recently, Porter and Smyth (2002) simulated the morning glory of the Gulf of Carpentaria, Australia, using numerical solution of the Benjamin–Ono equation. Their model indeed generated two solitary wavetrains propagating in two opposite directions on two sides of the topographic feature. Farmer and Armi (1999) and Armi and Farmer (2002) measured the behaviour of stratified water flow over bottom topography in Knight Inlet, British Columbia, Canada. Their measurements also showed that an upstream solitary wavetrain was indeed generated by the topography. Here we report a new case, which appears on satellite images and provides striking evidence of the coexistence of both upstream and downstream solitary wavetrains in the real atmosphere. In order to confirm this conclusion, we will also show the comparison between the observed case with theoretical models derived by Grimshaw and Smyth (1986).

2. Satellite images

The Sea-viewing Wide Field-of-view Sensor (SeaWiFS) onboard the Orbview-2 satellite is an eight-band (six visible and two near-infrared) optical scanner and was launched into a sun-synchronous orbit at an altitude of 705 km on 1 August 1997 (McClain *et al.* 1998). The images are produced by the National Aeronautics and Space Administration (NASA) Goddard Space Flight Center (GSFC) and distributed by the Distributed Active Archive Center (DAAC). There are two kinds of image products with different coverage for users' choices: Local Area Coverage (LAC) SeaWiFS images with a swath width of 2801 km and a spatial resolution at nadir of 1.1 km, and Global Area Coverage (GAC) SeaWiFS images with a swath width of 1502 km and a spatial resolution at nadir of 4.5 km. The images used for this study are LAC images.

3. Interpretation

The case of interest is shown in figure 1. Previous studies suggest that all undular cloud patterns represent signatures of atmospheric waves (Zheng *et al.* 1998a; Eckermann and Preusse 1999, Li *et al.* 2001). A digitally orthorectified version of figure 1 (in black and white and not shown here) was used to obtain accurate measurements of the phenomena. The packet stretching southward from the island (P_1) contains 23 waves. The concave orientation of the wave cloud lines in P_1 implies that the wave packet propagates southward. The average separation distance (or wavelength) between solitons is 6.4 km. The maximum length of the crest lines is 330 km. The packet located north-eastward 200 km off the north-east coast of the island (P_2) contains more than 20 waves. The concave orientation of the wave cloud lines in P_2 again implies that the wave packet propagates northward. The average wavelength of the first 10 solitons is 9.8 km. The maximum length of crest lines is 370 km. Figure 2 shows charts of sea surface pressure and wind velocity (upper) and geopotential height and velocity at 850 mbar (lower) on the same date and indicates a low pressure centre moving south-eastward from South China toward the study area. At the sea surface, the wind is southerly at 5 m s^{-1} . At 850 mbar, it is south-westerly and around 10 m s^{-1} . These observations

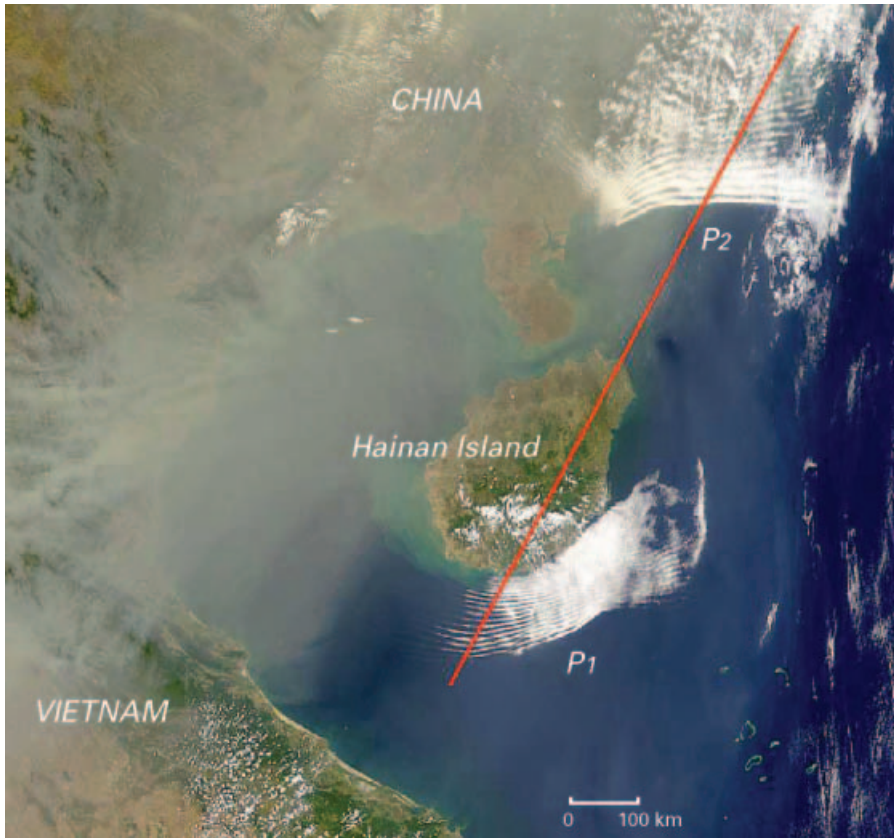


Figure 1. A true colour SeaWiFS image taken on 19 March 1999. The waters of the northern South China Sea are shown in dark blue. Aerosol contamination is evident to the west of the Hainan Island. Two groups of wave clouds in white arrayed on the two sides of the island are interpreted as signatures of upstream (P_1) and downstream (P_2) solitary wavetrains generated in the real atmosphere by topographic disturbances. The red line represents the wind direction at 850 mbar.

provide additional evidence that wave packet P_1 propagates upstream and P_2 downstream, respectively.

Figure 3 shows a cross-section taken along the red line in figure 1. Shown at the bottom of the figure is the topography of Hainan Island with a $1/12^\circ$ by $1/12^\circ$ resolution. Most of the island is covered by the Wuzhi Mountain with a peak at 1867 m above sea level located at $109^\circ 42' E$, $18^\circ 54' N$ near the centre of the island. Shown at the top of the figure are the grey value curves of the wave clouds. The grey values are related to cloud top altitudes, but are not calibrated. In figure 3, P_1 is just in front of a steep topographic elevation rising from the ocean surface, which constitutes a sudden obstruction in the way of the airflow, producing favourable conditions for generating upstream solitons. P_2 is distributed on the downstream side located 200 km off the coast of the island.

4. Comparison with theoretical models

In order to confirm the relationship between the two coexisting atmospheric wave packets shown on figure 1 and to determine their dynamical features, we

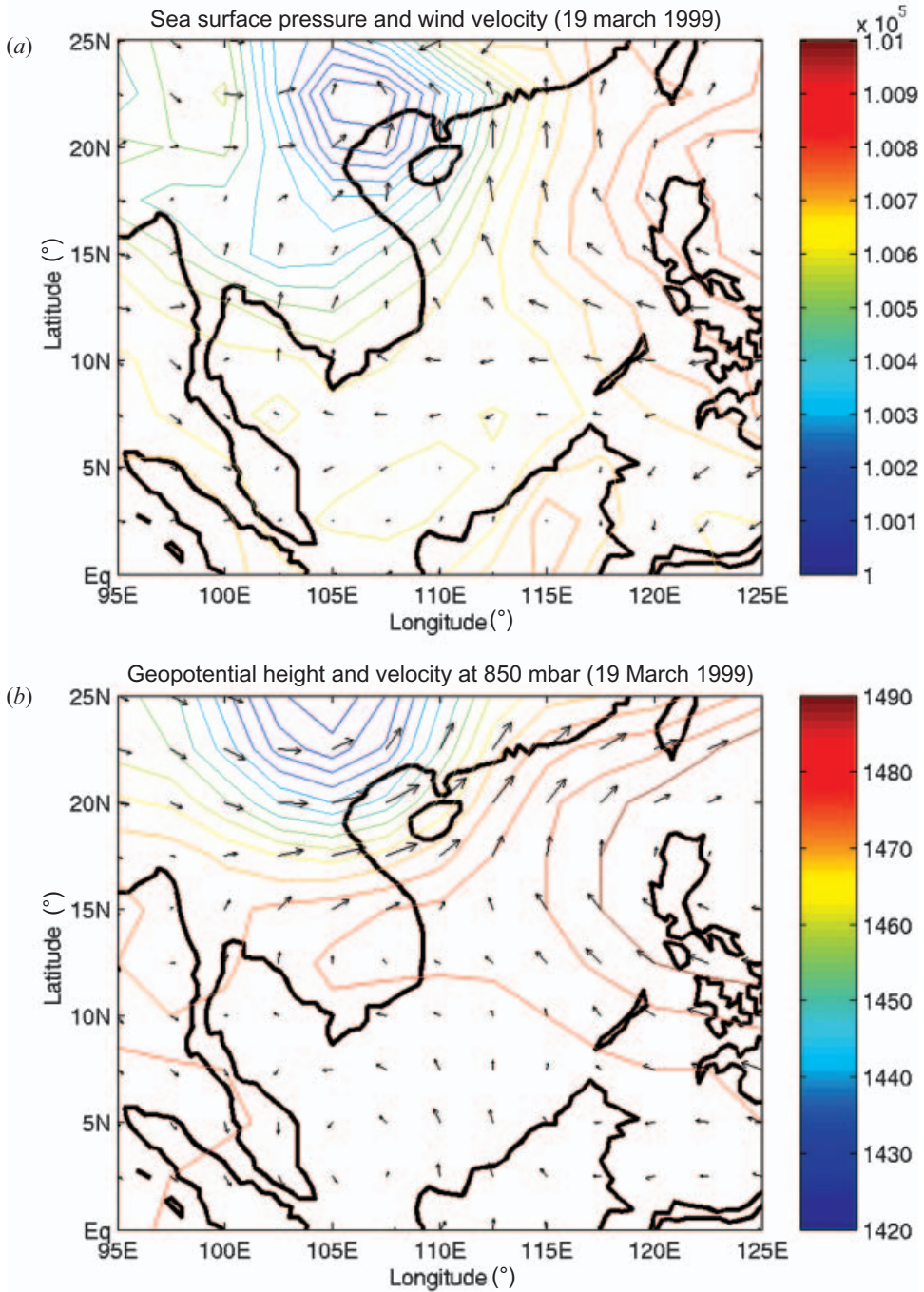


Figure 2. Weather charts for the observation area on 19 March 1999 (National Centers for Environmental Prediction Reanalysis data taken from the NOAA web site). (a) Sea surface pressure and wind velocity. The units of the colour code are Pascals. Arrows represent the wind field. In the study area, the sea surface wind is southerly and about 5 m s^{-1} . (b) Geopotential height and wind velocity at 850 mbar isobaric level. The units of the colour code are metres. Arrows represent the wind field. In the study area, the wind is south-westerly and about 10 m s^{-1} .

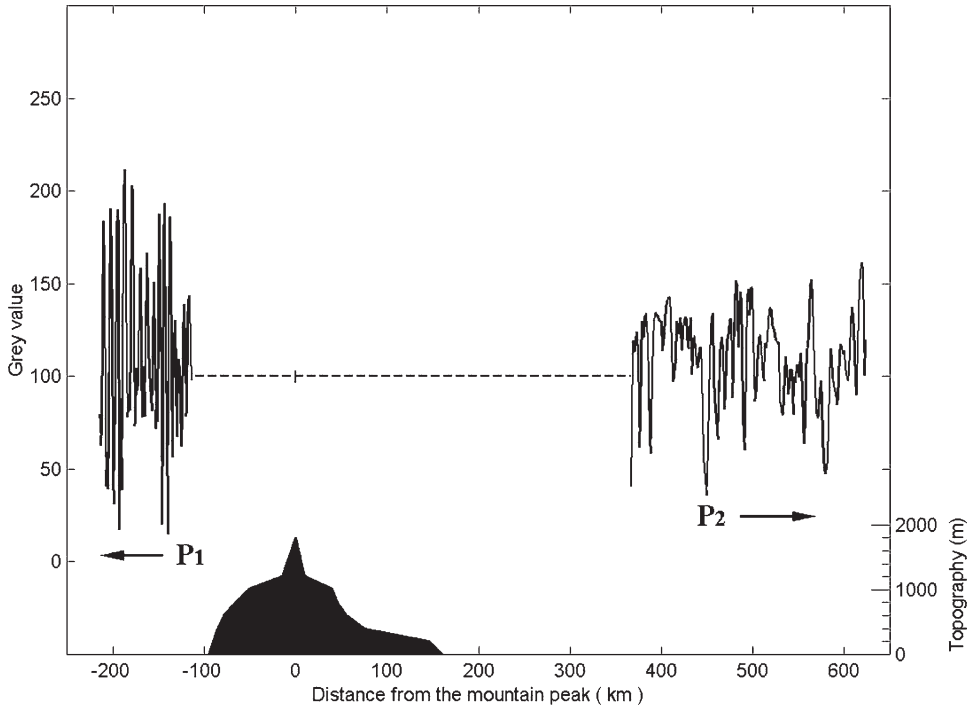


Figure 3. Cross-section along the red line shown in figure 1. The topography of Hainan Island (extracted from ETOPO5 5' × 5' Navy bathymetry data taken from US Navy web site) is shown at the bottom. The grey value curves of wave packets P₁ and P₂ with arrows showing the propagation directions are shown at the top.

decided to compare the observed case with available theoretical results. In the non-resonant case of continuously stratified flow of an inviscid incompressible fluid over topography, Grimshaw and Smyth (1986) found a wave motion solution in the form of

$$A_s = -\frac{c_s^2}{c_s^2 - V^2} G_s(X) + \frac{c_s}{2c_s^+} G_s(X - c_s^+ T) + \frac{c_s}{2c_s^-} G_s(X + c_s^- T), \text{ for } 0 < T < \infty \quad (1)$$

where $c_s = 2Nh/\pi$, in which N is the Brunt–Väisälä frequency and h is the vertical dimension of the waveguide, and is the long-wave phase speed relative to a basic state at rest, V is a constant horizontal velocity from left to right, $G_s(X)$ is the normalized background topography, $c_s^\pm = c_s \pm V$, $G_s(X - c_s^+ T)$ and $G_s(X + c_s^- T)$ represent two coexisting, freely propagating long waves, respectively, X is the slow space variable positive right, and T is the slow time variable. Those waves $G_s(X - c_s^+ T)$ with phase speed c_s^+ propagate downstream, while those waves $G_s(X + c_s^- T)$ with speed c_s^- propagate upstream for subcritical flow, $V < c_s$, and propagate downstream for supercritical flow, $V > c_s$. This solution is derived based on the following assumptions of length-scales: (a) the amplitude of the topography to be much less than the vertical dimension of the waveguide; (b) the wave amplitude to be much less than the vertical dimension of the waveguide; and (c) the horizontal length-scale of the topography to be much greater than the vertical dimension of the waveguide. The solution also predicts that, on a long timescale, the freely propagating waves will be affected by non-linearity and dispersion, and

will evolve either into a finite number of solitary waves, or into an oscillatory wavetrain.

In our case, the topography is imposed by Hainan Island. The horizontal length-scale of the island is 250 km and the average amplitude of a mountain ridge along 19° N is 600 m. The satellite image (figure 1) shows bands of clouds forming large clusters, 300–400 km in extent. The morphology of these features indicates that the clouds are stratocumulus, a sort of low-level cloud with the cloud top height lower than 3 km (Kidder and Vonder Haar 1995). This implies that the vertical dimension of the waveguide is less than 3 km. Cloud images have solitary wave packet features the same as the case observed in the north Arabian Sea (Zheng *et al.* 1998a). Hence, according to classification of atmospheric solitary waves by Rottman and Grimshaw (2002), the waves we observed belong to the class of low-level solitary waves. The length-scales of our case meet assumption (c), probably meet assumption (a), but do not include the wave amplitude scale. Here we consider assumption (b) to be met so that we may compare our case with theoretical solution (1). On the basis of solution (1), our case should be generated by subcritical flow, because a wave packet propagates upstream and another downstream, simultaneously. If the two wave packets coexist, in other words they were generated at the same time, the following relation must be true:

$$\frac{L_u}{c_s^-} = \frac{L_d}{c_s^+} \quad (2)$$

where L_u and L_d are upstream and downstream distances from the mountain ridge to the upstream and downstream packets, respectively. From the digitally orthorectified version of figure 1 (not shown here), we measure $L_u=140$ km and $L_d=370$ km. Substituting these value into (2) yield

$$\frac{c_s^+}{c_s^-} = \frac{c_s + V}{c_s - V} = 2.64 \quad (3)$$

From figure 2, we determine $V=10$ m s⁻¹. Thus, we obtain $c_s/V=2.2$, and $c_s=22$ m s⁻¹. Both the ratio c_s/V and the value of c_s are close to that of morning glory cases (Rottman and Grimshaw 2002). In other words, they are within a reasonable range. Therefore, we believe that relation (2) stands in our case. This confirms the coexistence of upstream and downstream solitary wavetrains.

Solution (1) also gives the normalized amplitudes of upstream (A_u) and downstream (A_d) solitary wavetrains. Substituting values of c_s , c_s^+ and c_s^- into (1) yields $A_u=1.83$, and $A_d=0.69$. Although we can determine the ratio of these amplitudes based on satellite images, we cannot determine their absolute values. The amplitude of a soliton is inversely proportional to the square of the characteristic half width (Zheng *et al.* 2001), and the latter is directly proportional to the width of a cloud image line no matter what imaging mechanisms. Therefore, the ratio of A_u and A_d , a_{ud} , can be estimated from the satellite image. In our case we measure the average image width of leading soliton of upstream wavetrain as 3.5 km, and that of the last soliton of downstream wavetrain as 5.6 km, thus $a_{ud}=2.6$. On the other hand, the theories give a_{ud} as 2.65. Both values are almost the same. This further confirms the coexistence of upstream and downstream solitary wavetrains.

Using the above data, we calculated the generation time of the waves as of 3.2 h earlier. The vertical dimension of a waveguide can be calculated using $h = \pi c_s / 2N$. If we take the Brunt–Väisälä frequency N as 0.02 s⁻¹, a typical value for the low-level

atmosphere (Rottman and Grimshaw 2002), we obtain an estimate for h of 1.7 km, which is close to the cases of morning glory (Noonan and Smith 1985). We also obtain an estimate for the Froude number (V/Nh) of 0.3, implying subcritical flow in this case.

5. Conclusions

From SeaWiFS satellite images we observed two packets of orderly wave clouds on two sides of Hainan Island in the South China Sea. Weather charts and the concave orientations of the wave cloud lines imply that the packets propagate both upstream and downstream in the wind direction simultaneously. Our observation and interpretation are well supported by the wave solutions derived by Grimshaw and Smyth (1986). Therefore, we conclude that this case provides evidence for the coexistence of upstream and downstream solitary wavetrains generated in the real atmosphere by topographic disturbances.

Acknowledgments

This research was supported partially by the National Aeronautics and Space Administration (NASA) through Grant NAG5-12745, by the Office of Navy Research (ONR) through Grant N00014-03-1-0337, by the National Oceanic and Atmospheric Administration (NOAA) through Grant NA17EC2449, and NOAA Sea Grant through NA03OAR4170011.

References

- ARMI, L., and FARMER, D., 2002, Stratified flow over topography: bifurcation fronts and transition to the uncontrolled state. *Proceedings of the Royal Society of London Series A*, **458**, 513–538.
- ECKERMANN, S. D., and PREUSSE, P., 1999, Global measurements of stratospheric mountain waves from space. *Science*, **286**, 1534–1537.
- FARMER, D., and ARMI, L., 1999, Stratified flow over topography: the role of small-scale entrainment and mixing in flow establishment. *Proceedings of the Royal Society London A*, **455**, 3221–3258.
- CHUNCHUZOV, I., VACHON, P. W., and LI, X., 2000, Analysis and modeling of atmospheric gravity waves observed in RADARSAT SAR images. *Remote Sensing of Environment*, **74**, 343–361.
- GRIMSHAW, R. H. J., and SMYTH, N., 1986, Resonant flow of a stratified fluid over topography. *Journal of Fluid Mechanics*, **169**, 429–464.
- KIDDER, S. G., and VONDER HAAR, T. H., 1995, *Satellite Meteorology* (San Diego: Academic Press), pp. 164–166.
- LI, X., CLEMENTE-COLÓN, P., PICHEL, W. G., and VACHON, P. W., 2000, Atmospheric vortex streets on a RADARSAT SAR image. *Geophysical Research Letters*, **27**, 1655–1658.
- LI, X., ZHENG, Q., PICHEL, W. G., YAN, X.-H., LIU, W. T., and CLEMENTE-COLÓN, P., 2001, Analysis of coastal lee waves along the coast of Texas observed in advanced very high resolution radiometer images. *Journal of Geophysical Research*, **106**, 7017–7025.
- LI, X., DONG, C., CLEMENTE-COLÓN, P., PICHEL, W. G., and FRIEDMAN, K., 2004, Synthetic aperture radar observation of the sea surface imprints of upstream atmospheric solitons generated by flow impeded by an island. *Journal of Geophysical Research*, **109**, C02016, doi: 10.1029/2003JC002168.
- MCCLAINE, C. R., CLEAVE, M. L., FELDMAN, G. C., GREGG, W. W., and HOOKER, S. B., 1998, Science quality SeaWiFS data for global biosphere research. *Sea Technology*, **39**, 10–15.
- NOONAN, J. A., and SMITH, R. K., 1985, Linear and weakly nonlinear internal wave theories applied to ‘morning glory’ waves. *Geophysical and Astrophysical Fluid Dynamics*, **33**, 123–143.

- PORTER, A., and SMYTH, N. F., 2002, Modeling the morning glory of the Gulf of Carpentaria. *Journal of Fluid Mechanics*, **454**, 1–20.
- ROTTMAN, J. W., and GRIMSHAW, R., 2002, Atmospheric internal solitary waves. *Environmental Stratified Flows*, edited by R. Grimshaw (Boston: Kluwer Academic Publishers), pp. 61–88.
- SHEN, S. S. P., 1993, *A Course on Nonlinear Waves* (London: Kluwer Academic Publishers), pp. 147–187.
- VACHON, P. W., JOHANNESSEN, O. M., and JOHANNESSEN, J. A., 1994, An ERS-1 synthetic aperture radar image of atmospheric lee waves. *Journal of Geophysical Research*, **99**, 22483–22490.
- WU, T. Y.-T., 1987, Generation of upstream advancing solitons by moving disturbances. *Journal of Fluid Mechanics*, **184**, 75–99.
- ZHENG, Q., YAN, X.-H., LIU, W. T., KLEMAS, V., GREGER, D., and WANG, Z., 1998a, A solitary wave packet in the atmosphere observed from space. *Geophysical Research Letters*, **25**, 3559–3562.
- ZHENG, Q., YAN, X.-H., LIU, W. T., KLEMAS, V., HO, C.-R., KUO, N.-J., and WANG, Z., 1998b, Coastal lee waves on ERS-1 SAR images. *Journal of Geophysical Research*, **103**, 7979–7993.
- ZHENG, Q., YUAN, Y., KLEMAS, V., and YAN, X.-H., 2001, Theoretical expression for an ocean internal soliton SAR image and determination of the soliton characteristic half width. *Journal of Geophysical Research*, **106**, 31415–31423.